MALAYSIAN JOURNAL OF MICROSCOPY

Journal homepage: https://malaysianjournalofmicroscopy.org

RESEARCH ARTICLE

UTILIZATION OF NATURAL SILICA FROM RICE HUSK ASH TO IMPROVE ELECTRICAL CONDUCTIVITY OF SDC-BASED IT-SOFC ELECTROLYTE

Zolhafizi Jaidi[1], Mohd Azham Azmi[1,*], Hamimah Abd Rahman[1], Nurul Farhana Abdul Rahman[1], Nor Suzyliana Ahmad[2], Wan Hasrulnizzam Wan Mahmood[3], Hadi Abdul Salaam[4], Ahmad Husni Mohd Shapri[5]

[1] Faculty of Mechanical and Manufacturing Engineering, Universiti Tun Hussein Onn Malaysia, 86400 Parit Raja, Batu Pahat, Johor, Malaysia.
[2]Department of Electronic Technology, Kolej Vokasional Batu Pahat, Jalan Kluang, 83000 Batu Pahat, Johor, Malaysia.
[3]Faculty of Industrial & Manufacturing Technology & Engineering, Universiti Teknikal Malaysia Melaka, Jalan Hang Tuah Jaya, 76100 Durian Tunggal, Melaka, Malaysia.
[4]Faculty of Mechanical and Automotive Engineering Technology, Universiti Malaysia Pahang Al-Sultan Abdullah 26600 Pekan Pahang, Malaysia.
[5]Faculty of Electronic Engineering and Technology, Universiti Malaysia Perlis, 02600 Arau Perlis, Malaysia.

Abstract. Solid oxide fuel cells (SOFCs) rely on electrolytes with high ionic conductivity and thermal stability, especially for intermediate-temperature operations (500–700 °C). Yttria-stabilized zirconia (YSZ), the conventional SOFC electrolyte, requires high operating temperatures, which leads to thermal mismatch, interfacial degradation, and other performance issues. Samarium-doped ceria (SDC) is a promising alternative due to its superior ionic conductivity at lower temperatures. However, SDC still faces challenges in achieving full densification and minimal porosity without elevated sintering temperatures. This study explores the incorporation of natural silica derived from rice husk ash ($RHASiO_2$) as an eco-friendly sintering aid to enhance the structural and electrochemical performance of SDC electrolytes. $RHASiO_2$ was calcined at 700 °C and combined with commercial SDC powder in various weight percentages (0 %–3 %) using dry ball milling. The mixtures were uniaxially pressed into pellets and sintered at 1200 °C. Thermogravimetric analysis (TGA) showed that $RHASiO_2$ improved thermal stability by reducing weight loss during intermediate and final degradation phases. The microstructure and morphology were characterized using scanning electron microscopy (SEM), while porosity was quantified through image analysis using ImageJ software. The results revealed a decreasing trend in porosity with increasing $RHASiO_2$ content, reaching the lowest value of 4.58 % in the SDC3.0 sample. Electrochemical impedance spectroscopy (EIS) demonstrated enhanced conductivity and reduced grain boundary resistance for $RHASiO_2$-modified samples. The highest total ionic conductivity, 2.76×10^{-2} $S \cdot cm^{-1}$ at 700 °C, was achieved by SDC3.0, which also exhibited the lowest activation energy of 0.768 eV. These results confirm that $RHASiO_2$ effectively promotes densification and enhances the electrical conductivity of SDC electrolytes, offering a sustainable and low-cost route to improve SOFC performance.

Keywords: Samarium-doped ceria (SDC), rice husk ash silica ($RHASiO_2$), solid oxide fuel cell (SOFC), electrochemical impedance spectroscopy (EIS), sintering aid.

Article Info

Received 10 January 2026
Accepted 23 April 2026
Published 8 June 2026

***Corresponding author: azham@uthm.edu.my**

ISSN: 1823-7010, eISSN: 2600-7444

1. INTRODUCTION

Solid oxide fuel cells (SOFCs) rely heavily on the performance of their electrolytes, which serve as a medium for oxide ion conduction. Among the key parameters, ionic conductivity is the most critical property of solid oxide electrolytes [1]. YSZ is the most widely used electrolyte in conventional SOFCs due to its chemical stability and mechanical robustness. However, YSZ requires high operating temperatures (800–1000 °C) to achieve adequate ionic conductivity (~0.01 S/cm), leading to several material challenges such as thermal expansion mismatches between components, electrode coking, interfacial diffusion, and difficulties in achieving reliable cell sealing [2,3]. As an alternative, ceria-based electrolytes, particularly SDC, have emerged as promising candidates for intermediate-temperature SOFCs (IT-SOFCs, 500–700 °C) due to their superior ionic conductivity in this range [4]. Previous studies have reported that SDC exhibits conductivity in the range of 10^{-3} to 10^{-2} $S \cdot cm^{-1}$ at 600–700 °C, mainly due to the formation of oxygen vacancies from Sm^{3+} substitution in the ceria lattice. In addition, SDC shows good compatibility with electrode materials, further improving its electrochemical performance. However, challenges such as incomplete densification and possible electronic conduction under reducing conditions still limit its performance [5,6].

In recent years, the incorporation of silica (SiO_2) as a sintering aid has been widely explored to reduce the sintering temperature and enhance the densification of ceria-based electrolytes. Among various silica sources, rice husk ash (RHA) has emerged as a promising natural precursor due to its high silica content (typically >85–95 wt%), amorphous structure, low cost, and abundant availability as an agricultural waste by-product. Compared to conventional commercial silica, RHA-derived silica offers advantages such as higher reactivity, finer particle size after processing, and environmental sustainability. Previous studies have demonstrated that RHA-derived silica can improve densification and reduce sintering temperature; however, several limitations remain, including insufficient control of microstructural homogeneity, limited analysis on conductivity enhancement mechanisms, and lack of optimization of silica content, which may lead to excessive grain boundary resistance when used in higher amounts [7].

The addition of silica must therefore be carefully controlled. While low silica content can promote liquid-phase sintering and improve grain packing, excessive silica may segregate at grain boundaries, forming insulating phases that hinder oxide ion transport [8,9]. In this study, the silica content was limited to a maximum of 3.0 wt% to balance densification and ionic conductivity. This selection is based on prior findings indicating that silica content beyond this threshold tends to increase grain boundary resistance and reduce overall conductivity. Investigating this compositional range allows the study to identify the optimal trade-off, while also providing insight into the potential impact of higher silica content, which is expected to negatively affect electrochemical performance due to phase segregation and blocking effects.

In addition, a modified ball-milling approach was employed to improve powder homogeneity and particle size distribution. Unlike conventional ball-milling, the modification in this study involves extended milling duration, controlled milling speed, and optimized ball-to-powder ratio, which collectively enhance particle refinement and ensure uniform dispersion of RHA-derived silica within the SDC matrix. This modification is critical to achieving better mixing at the nanoscale level, thereby promoting uniform densification and minimizing agglomeration during sintering [10].

Despite numerous studies utilizing RHA as a sintering aid, the novelty of this work lies in the systematic integration of controlled low-percentage RHA-derived silica with an optimized powder processing route to achieve enhanced electrolyte performance. Unlike previous reports that primarily focus on densification behavior, this study provides a comprehensive evaluation of both microstructural and electrochemical properties, particularly emphasizing the correlation between silica content, grain boundary characteristics, and ionic conductivity. Furthermore, this work addresses the gap in understanding the optimal silica loading and its influence on conductivity degradation at higher concentrations [4].

EIS was employed to characterize the electrochemical properties of the sintered SDC–$RHASiO_2$ samples. EIS is a powerful technique that provides detailed insights into various polarization phenomena within SOFC systems, including ohmic, activation, and concentration losses [11]. By applying an alternating current over a wide frequency range, the impedance response can be analyzed through Nyquist plots, where the high-frequency intercept represents the bulk resistance, and the low-frequency intercept corresponds to the total resistance. This enables the separation of grain interior and grain boundary contributions, which is essential for understanding the effect of silica addition on ionic transport [12].

Therefore, this study aims to investigate the role of RHA-derived SiO_2 as a sustainable and cost-effective sintering aid in enhancing the densification and ionic conductivity of SDC-based electrolytes. By systematically evaluating compositions up to 3.0 wt% SiO_2 and employing an improved powder processing technique, this work provides new insights into optimizing electrolyte performance while addressing the limitations of previous studies.

2. MATERIALS AND METHODS

2.1 Silica production from rice husk

$RHASiO_2$ was produced from rice husk waste collected from a rice milling facility in Muar, Johor, Malaysia. The rice husks were initially subjected to uncontrolled open-air combustion at the milling site, generating rice husk ash at an estimated temperature of approximately 450 °C. The resulting ash, which contained silica along with residual carbonaceous components and trace impurities, appeared as a greyish powder. To enhance silica purity and eliminate remaining organic residues, the collected ash was further calcined in a muffle furnace at 700 °C. This thermal treatment facilitated the oxidation of residual carbon and promoted the formation of amorphous silica structures commonly found in rice husk ash–derived materials. Following calcination, the $RHASiO_2$ powder was subjected to particle size refinement using a dry ball-milling process for 3 hours. This process reduced particle agglomeration and produced a relatively uniform particle size distribution within the range of approximately 0.1–0.6 μm. The processed silica powder was then stored in sealed containers to minimize contamination and moisture absorption prior to further processing.

2.2 Characterizations of composite powder

Commercial SDC powder supplied by Kceracell (Korea) was used as the primary electrolyte material for composite preparation. The $RHASiO_2$ additive was blended with SDC powder using a low-speed ball-milling technique to ensure homogeneous dispersion of silica particles within the ceria matrix. The mixing process was performed at a rotational speed of 200 rpm for 3 hours. A series of SDC–$RHASiO_2$ composite powders were prepared by varying the silica additive content relative to SDC. The compositions were designated as SDC0 (0 wt%), SDC0.25 (0.25 wt%), SDC0.5 (0.5 wt%), SDC1.0 (1.0 wt%), SDC2.0 (2.0 wt%), and SDC3.0 (3.0 wt%). The homogenized powders were subsequently compacted into disc-shaped pellets using a uniaxial hydraulic press. The pellets were fabricated with a diameter of 30 mm and an approximate thickness of 1 mm. This compaction step ensured sufficient green density and structural integrity prior to sintering. All pellets were sintered at 900 °C, 1000 °C, 1100 °C and 1200 °C for 60 minutes with heating rate 10 $°C.min^{-1}$ in a high-temperature furnace to promote densification and microstructural development of the electrolyte materials. The sintered samples were then allowed to cool naturally to room temperature before being subjected to further characterization and electrochemical evaluation.

The thermal behavior and decomposition characteristics of the synthesized SDC–$RHASiO_2$ composite powders were investigated using simultaneous Differential Thermal Analyzer and Thermogravimetric Analyzer (DTA-TGA, Model: SDT2960). The measurements were conducted under ambient air atmosphere with a heating rate of 10 °C min^{-1} from room temperature to the desired temperature range. TGA data provided quantitative information on weight loss associated with moisture

removal, decomposition of organic residues, and volatilization of residual components. The microstructural morphology of the rice husk ash–derived silica and sintered electrolyte samples was examined using a scanning electron microscope (SEM, Hitachi SU1510, Japan). Quantitative porosity analysis was performed using ImageJ image-processing software based on the acquired SEM micrographs. High-resolution thin-section images of the pellet surface were selected to ensure accurate representation of the pore distribution within the material. Image processing steps included grayscale conversion, contrast enhancement, and threshold segmentation to clearly distinguish pore regions from the solid matrix. The porosity percentage was then calculated by determining the ratio of pore area to the total image area, allowing for improved accuracy and reproducibility in the porosity measurement.

The conductivity of the sintered SDC–$RHASiO_2$ electrolyte pellets was evaluated using EIS. The measurements were carried out using an Autolab electrochemical workstation (Metrohm, Switzerland) integrated with a high-temperature tube furnace. Prior to measurement, platinum mesh electrodes were attached to both sides of the electrolyte pellets to serve as current collectors and ensure stable electrical contact. The impedance spectra were recorded over a frequency range of 0.01 Hz to 1 MHz using an AC signal amplitude of 0.01 mV. The conductivity measurements were performed within a temperature range of 500 °C to 700 °C to simulate the operating conditions of IT-SOFCs. Each sample was maintained at the target temperature for at least 30 minutes prior to measurement to ensure thermal equilibrium and stabilization of the electrochemical response. The applied current ranged from 10 µA to 1 A depending on the impedance characteristics of the sample. The obtained impedance spectra were analyzed and fitted using NOVA 2.1 software to determine the bulk resistance and grain boundary resistance of the electrolyte materials. The ionic conductivity was subsequently calculated using the standard relationship between sample geometry and measured resistance.

3. RESULTS AND DISCUSSION

The novelty of this work is highlighted by the use of natural $RHASiO_2$ as a sustainable and low-cost silica source, together with the identification of an optimal low silica content (≤3 wt%) that balances densification and ionic conductivity. This study demonstrates simultaneous improvements in thermal stability, microstructural densification, and electrochemical performance, while providing clearer insight into the roles of grain boundary and bulk transport mechanisms. In contrast to previous studies that often address these aspects separately, the present work establishes a comprehensive correlation between porosity, impedance behavior, and conductivity, and further discusses the limitations associated with excessive silica addition, particularly its impact on grain boundary resistance and overall electrolyte performance.

3.1 Thermal Characterization (TGA) of SDC-$RHASiO_2$

TGA was employed to evaluate the thermal decomposition behavior and weight loss characteristics of SDC-$RHASiO_2$ composite powders, with results summarized in Table 1 and illustrated in Figure 1. The sintering temperatures of 900 °C, 1000 °C, 1100 °C, and 1200 °C do not represent separate sintering experiments, but rather selected data extraction points from a single continuous TGA heating profile. These points were used to simulate the effect of sintering temperatures on mass stability. The analysis covered six compositions (SDC0, SDC0.25, SDC0.5, SDC1.0, SDC2.0, and SDC3.0) each demonstrating distinct weight loss trends corresponding to increasing $RHASiO_2$ content. The TGA curves were interpreted across three degradation phases: initial (room temperature to 400 °C), intermediate (400–800 °C), and final (800–1300 °C). The initial phase showed mass loss due to water evaporation, particularly in the SDC0 sample, while the intermediate phase reflected decomposition of organic content and partial burning of SDC. The final degradation stage involved oxidation of residual organics and structural transitions within the ceria lattice, further influenced by the incorporation of silica from $RHASiO_2$. These phase transitions, driven by increasing temperature, are strongly associated with changes in crystallinity and porosity, indicating that the Si element plays a vital role in enhancing thermal stability and reducing weight loss by stabilizing the composite structure during sintering [13].

The graph was also plotted to identify the weight loss of four different sintering temperatures, which are 900 °C, 1000 °C, 1100 °C and 1200 °C which can be observed as the sintering temperature increases, the weight loss will increase. The amount of weight loss for all samples is shown in Table 1. The weight loss happened through a process of heating rate.Through initial degradation shows that 100 % SDC has the highest weight loss at a range of 0℃ to 400 ℃, with 0.2555 mg followed by SDC-$RHASiO_2$ 2 %, SDC-$RHASiO_2$ 3 %, and SDC-$RHASiO_2$ 1 % with 0.1454 mg, 0.1327 mg, and 0.0494 mg. Next phase, the intermediate phase was set at a range of 401 ℃ to 800 ℃ to see the weight loss of 4 different compositions of SDC-$RHASiO_2$ starting at temperatures 500℃-600 ℃. The highest weight loss in an intermediate phase is SDC-$RHASiO_2$ 3 % with losses of 0.0997 mg, and the lower weight loss is 100 % SDC with 0.0522 mg. The final degradation of the graph of thermogravimetric analysis shows the highest weight loss of the composition powder at 801 to 1300 ℃ because a lot of the composition powder has a melting point in that temperature range. At these temperatures, the SDC-$RHASiO_2$ 3 % lost a lot of weight at 0.2696 mg and was followed by SDC-$RHASiO_2$ 2 %, SDC-$RHASiO_2$ 1 %, and 100 % SDC with 0.2182 mg, 0.2063 mg, and 0.2058 mg.

Table 1: Weight loss of SDC-$RHASiO_2$ composite powder at 900 °C, 1000 °C, 1100 °C and 1200 °C

	Weight Loss (mg)			
Samples	Sintering Temperature (°C)			
	900	1000	1100	1200
SDC0	1.34	1.5	1.62	1.78
SDC0.25	0.86	1.11	1.24	1.36
SDC0.5	0.85	0.95	1.08	1.29
SDC1.0	0.78	0.81	0.86	0.93
SDC2.0	0.5	0.66	0.76	0.93
SDC3.0	0.61	0.69	0.74	0.86

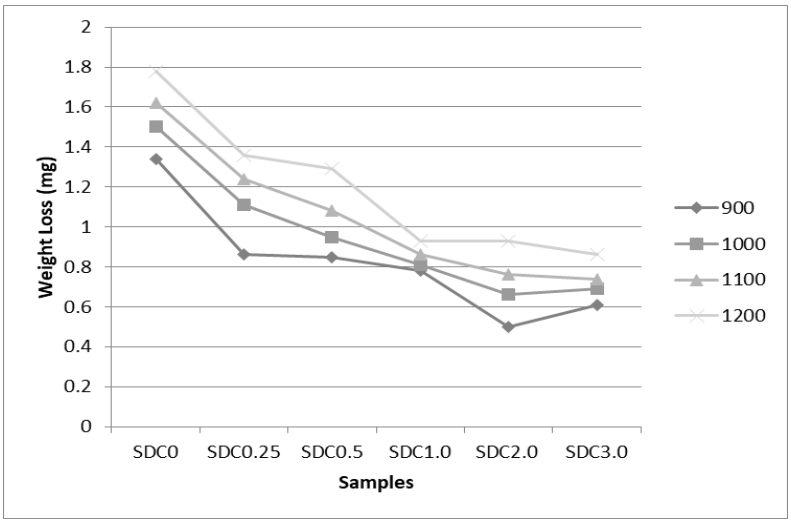

Figure 1: Weight loss of SDC-$RHASiO_2$ composite powder at sintering temperature of 900 °C, 1000 °C, 1100 °C and 1200 °C

The data presented in Table 1 and Figure 1 clearly demonstrate that the incorporation of $RHASiO_2$ into the SDC-$RHASiO_2$ composite enhances thermal stability, as evidenced by the overall reduction in weight loss with increasing $RHASiO_2$ content. This trend indicates that $RHASiO_2$ serves a

stabilizing role within the composite, counteracting the effects of thermal decomposition and volatilisation that are typically intensified at higher sintering temperatures. One possible explanation is that $RHASiO_2$ contributes to the formation of a denser and more thermally robust microstructure, which minimizes porosity and restricts the escape of volatile components, thereby helping the composite maintain its integrity under elevated temperatures [13]. Additionally, $RHASiO_2$ may promote phase stabilization by chemically interacting with other constituents to form thermodynamically stable phases that resist high-temperature breakdown. This effect could also help suppress the volatilisation of impurity phases or undesirable secondary compounds. Moreover, $RHASiO_2$ may act as a scavenger for impurities, reducing their concentration and further preventing thermally induced mass loss [14]. Weight loss due to the decomposition of organic additives or binders, which typically release gaseous by-products during heating, is also mitigated by the presence of $RHASiO_2$. Furthermore, volatilisation of intrinsic or processing-related impurities often a result of sintering conditions or raw material inconsistencies that can be reduced through $RHASiO_2$ interaction, ultimately enhancing the thermal resilience of the SDC-$RHASiO_2$ system [15].

Although absolute weight loss increases with temperature due to thermally activated processes, the relative thermal stability improves with $RHASiO_2$ addition, as evidenced by the lower overall weight loss in doped samples compared to pure SDC. This apparent contradiction can be explained by distinguishing between temperature-driven weight loss and composition-driven stability. $RHASiO_2$ promotes structural stability by forming a more compact network and reducing volatilisation pathways. Regarding possible redox effects, slight weight variations at high temperature may also be associated with partial reduction of Ce^{4+} to Ce^{3+} under local oxygen-deficient conditions. However, this effect is expected to be minimal under the present experimental conditions and does not dominate the observed trends. In terms of purity, rice husk ash (RHA) typically contains high silica content (>85–95 wt%) after calcination, with minor impurities such as K_2O and CaO [16]. These impurities can act as fluxing agents, promoting liquid-phase sintering and enhancing densification. Although XRD analysis was not included in this study, the improved densification and reduced porosity indirectly suggest that no detrimental secondary phases were formed at the studied compositions. Future work will include XRD to further confirm phase purity and structural stability.

3.2 Porosity of SDC-$RHASiO_2$

Porosity was evaluated from SEM micrographs using ImageJ software based on grayscale thresholding and area fraction analysis. To improve statistical reliability, multiple SEM images (at least 3–5 regions per sample) were analyzed and averaged. The top surface section image may be used to determine porosity to increase accuracy and precision. This improvement in the colour palette, along with higher resolution and more thorough photography of the microporosity, will result in an improvement in the true area that the computer would threshold as pore space. The porosity was coloured red to set it apart from the top surface as a whole in Image J. Red dots indicated the presence of porosity and holes in the SDC-$RHASiO_2$ composite electrolyte. Consequently, the porosity number will be more precise and consistent with the overall porosity of the samples [17–19].

Table 2 and Figure 2 present the porosity values of SDC-$RHASiO_2$ electrolyte samples sintered at 1200 °C and $RHASiO_2$ concentrations (0, 0.25, 0.5, 1.0, 2.0, and 3.0 wt%). This comprehensive dataset enables a thorough analysis of the relationship between $RHASiO_2$ content, sintering temperature, and porosity. The porosity values range from approximately 4.95 % to 4.58 %, with a general trend of decreasing porosity with increasing $RHASiO_2$ concentration.

Several variables contribute to the observed reduction in porosity as $RHASiO_2$ concentrations increase in SDC-$RHASiO_2$ electrolytes. One important element is the effect of $RHASiO_2$ on particle packing during sintering. $RHASiO_2$'s unique chemical and physical features, such as surface energy, atomic size, and crystal structure, may improve particle density. This tighter packing can minimise the void space within the material, resulting in lower porosity. Additionally, $RHASiO_2$ may inhibit grain growth, contributing further to porosity reduction. $RHASiO_2$ may function as a grain development

inhibitor, resulting in a finer-grained microstructure. Smaller grains tend to reduce porosity at grain boundaries, leading to a denser material. Impurities in the $RHASiO_2$ material, as well as secondary phases formed during sintering, may further impact the densification process. These contaminants can interact with the SDC matrix, influencing the sintering process and subsequent microstructure. Impurities, for example, may interfere with grain boundary movement, resulting in a denser material [20,21].

Table 2: Porosity of SDC-$RHASiO_2$ electrolyte

Temperature (°C)	Sample	Porosity (%)
1200	SDC0	4.95
	SDC0.25	4.94
	SDC0.5	4.89
	SDC1.0	4.75
	SDC2.0	4.64
	SDC3.0	4.58

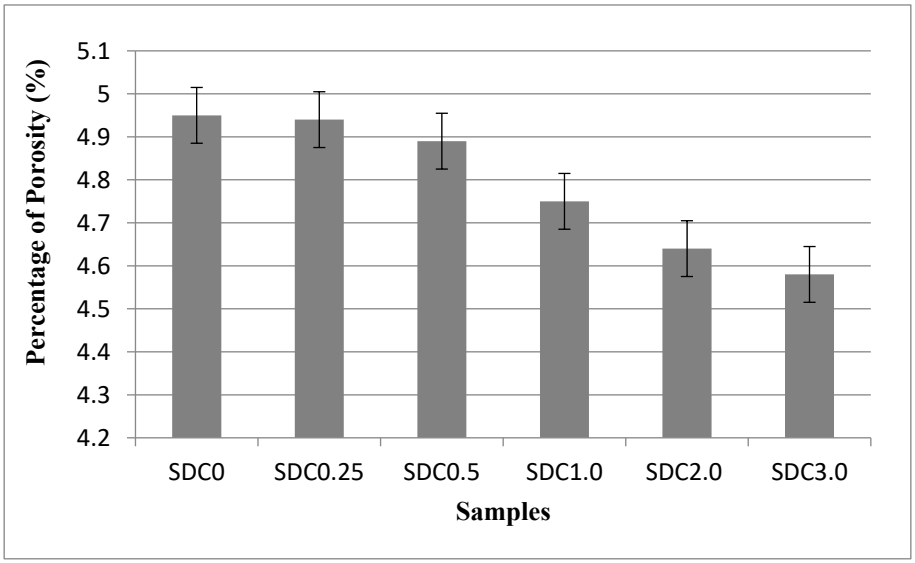

Figure 2: Graph of porosity of SDC-$RHASiO_2$ electrolyte

The results imply that adding $RHASiO_2$ to SDC-based electrolytes can dramatically reduce porosity. This is most likely owing to a mix of variables, including better particle packing, grain refining, and possible impurity effects. Based on the result obtained, the porosity percentage of SDC-$RHASiO_2$ pallets with 3wt% at 1200 °C showed the best result as the lowest porosity percentage. Figure 3 supports the findings. Although SDC3.0 shows the lowest porosity, it should be clarified that this does not necessarily represent the absolute optimum. Based on sintering theory, further increase (>3 wt%) is expected to result in silica segregation and formation of insulating grain boundary phases, which may trap pores or even increase effective porosity [8,9]. Therefore, 3 wt% is considered the optimal range within this study, not a universal maximum. Regarding the relatively small change in porosity (≈0.4 %), this difference is still significant in dense ceramic electrolytes. Even minor reductions in residual porosity can substantially improve ionic pathways and reduce grain boundary resistance, which is consistent with the observed conductivity enhancement. It should also be acknowledged that ImageJ analysis represents surface porosity estimation. While the results strongly indicate improved densification, future work incorporating bulk density measurements (e.g., Archimedes method) would further validate internal densification.

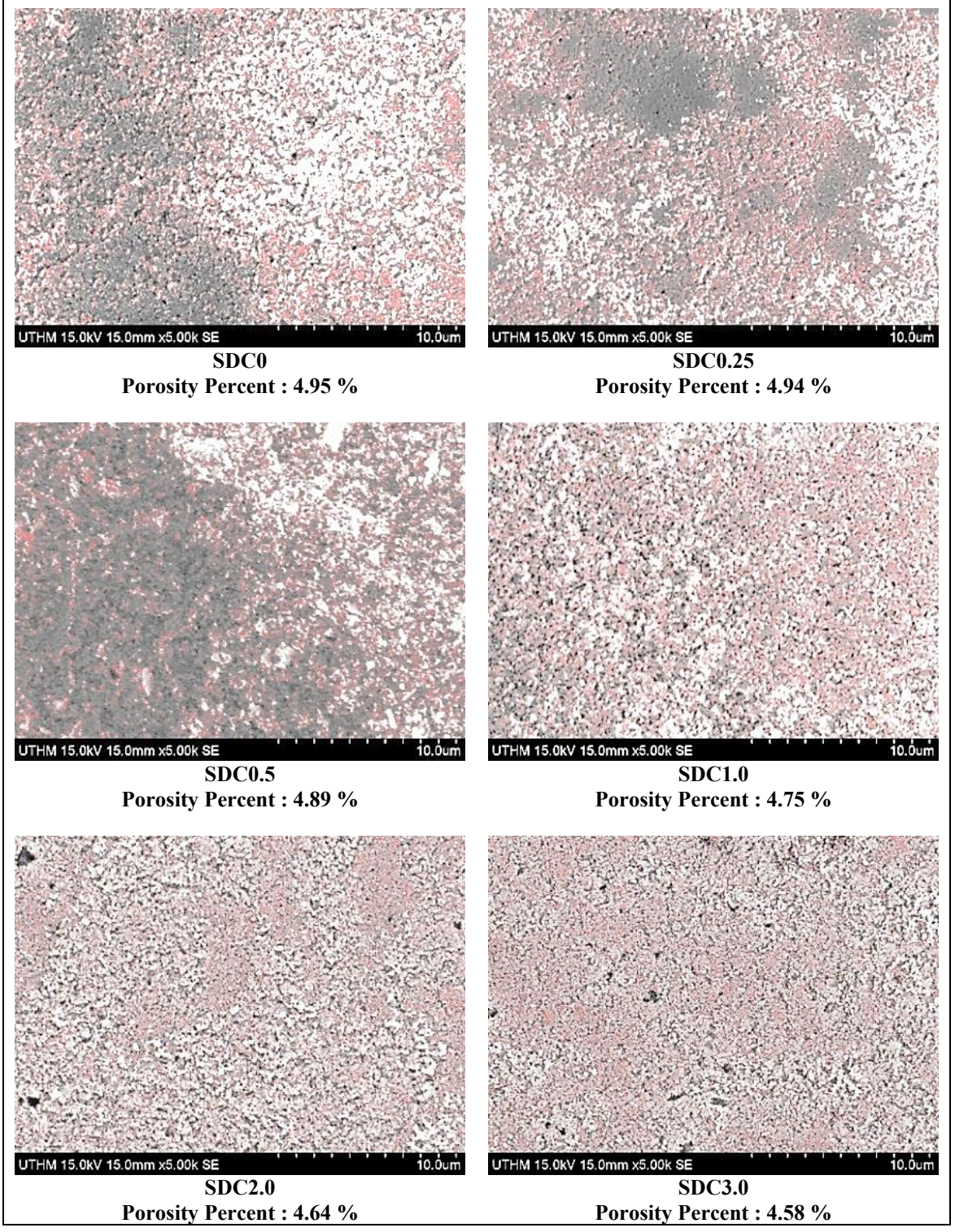

Figure 3: SEM images of surface morphology and porosity value through the ImageJ software for SDC-RHASiO_2 electrolyte at 1200 °C

3.3 Conductivity analysis of SDC-RHASiO$_2$

Figures 4, 5, and 6 present the EIS results of SDC-RHASiO$_2$ electrolytes measured at 500 °C. Ceria-based ceramics typically exhibit three distinct arcs in EIS spectra, corresponding to grain interior (HF), grain boundaries (MF), and electrode/electrolyte interface (LF) conduction processes. However, only two arcs were observed in this study, which can be attributed to the overlap or suppression of the high-frequency bulk response at elevated temperatures, where the associated relaxation time falls beyond the measurable frequency range of the instrument. The assignment of these arcs was validated through equivalent circuit modelling using the $R_0(R_1CPE_1)(R_2CPE_2)$ configuration, supported by comparison with reported literature and analysis of the capacitance values associated with each process. Based on this evaluation, the high-frequency arc is interpreted as a combined bulk response, while the mid-frequency arc corresponds to grain boundary conduction, indicating that the dominant contribution to impedance arises from grain boundary effects in the studied system.

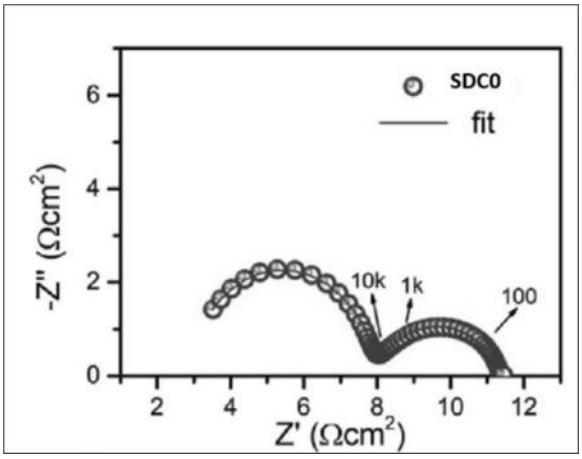

Figure 4: EIS results for SDC0 electrolytes measured at 500 °C

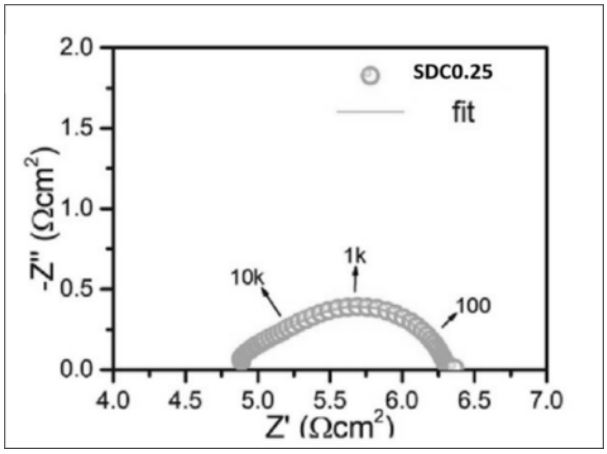

Figure 5: EIS results for SDC0.25 electrolytes measured at 500 °C

At elevated temperatures like 700 °C, the bulk conduction arc becomes less distinguishable due to reduced relaxation time beyond the analyser's detection limit (1 MHz), as reported in prior studies [22]. For example, the SDC0 sample (Figure 4) displays only two arcs, with the HF arc appearing increasingly truncated. To model the impedance behavior, the $R_0(R_1CPE_1)(R_2CPE_2)$ equivalent circuit was used, which is well-established for doped ceria systems [22]. This model, shown in Figure 7, includes constant phase elements (CPEs) to represent non-ideal capacitive behavior arising from distributed current paths and electroactive species [23]. The impedance spectra of the SDC0.25 sample

(Figure 5) show overlapping semicircles due to similar relaxation times, while the SDC3.0 sample (Figure 6) exhibits two clearly resolved arcs. Bulk resistance (Rb), grain boundary resistance (Rgb), and electrode/electrolyte interfacial resistance (Rel) were extracted from R_0, R_1, and R_2, respectively [24]. As shown in Figure 7, Rgb values for SDC0.25 and SDC3.0 dropped by nearly an order of magnitude compared to SDC0, indicating significantly improved grain boundary conductivity, while Rb showed a gradual increase with higher $RHASiO_2$ content.

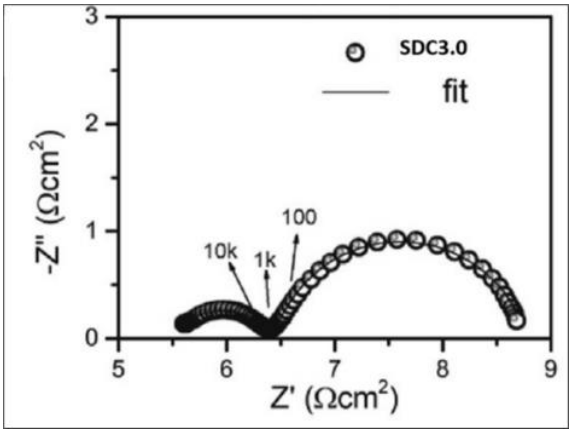

Figure 6: EIS results for SDC3.0 electrolytes measured at 500 °C

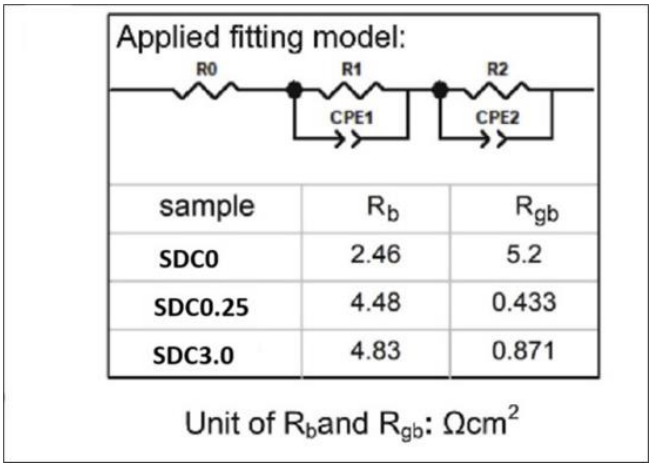

Figure 7: The $R_0(R_1CPE_1)(R_2CPE_2)$ model to fit the EIS data

Figure 8 shows the Arrhenius plots (ln dtT-1/T) for SDC-$RHASiO_2$ electrolytes measured between 500 °C and 700 °C, with total conductivity (dt) calculated using Equation 1,

$$dt = l/SRt, \quad (1)$$

where dt is total ionic conductivity ($S \cdot cm^{-1}$), Rt is total resistance obtained from EIS (Ω), *l* is the pellet thickness and *S* is the effective cross-sectional area. Total conductivities (*dt*) at 500 °C, 600 °C and 700 °C and conduction activation energy (Ea) in different electrolytes was tabulated in Table 3. At 500 °C, the total conductivity of the samples increased from 0.59 x 10^{-2} $S \cdot cm^{-1}$ (SDC0) to 0.77 x 10^{-2} $S \cdot cm^{-1}$ (SDC0.25) and further to 0.94 x 10^{-2} $S \cdot cm^{-1}$ (SDC3.0). A similar trend was observed at 600 °C, where conductivity rose from 1.21 x 10^{-2} $S \cdot cm^{-1}$ (SDC0) to 1.34 x 10^{-2} $S \cdot cm^{-1}$ (SDC0.25) and 1.72 x 10^{-2} $S \cdot cm^{-1}$ (SDC3.0). The enhancement became more pronounced at 700 °C, with SDC3.0 reaching 2.76 x 10^{-2} $S \cdot cm^{-1}$, surpassing both SDC0.25 (2.07 x 10^{-2} $S \cdot cm^{-1}$) and the undoped SDC0 (1.96 x 10^{-2} $S \cdot cm^{-1}$). This enhancement is attributed to a substantial reduction in grain boundary resistance (Rgb), facilitated by

finer grain structures that increase boundary area and dilute impurity effects, thus improving ionic transport. The slight increase in bulk resistance (Rb) with $RHASiO_2$ addition can be attributed to the intrinsically insulating nature of silica, which may partially block ionic transport within grain interiors. However, this negative effect is outweighed by the significant reduction in grain boundary resistance (Rgb) due to improved densification and reduced porosity. Activation energy (Ea) values further support these findings, decreasing from 0.898 eV in SDC0 to 0.796 eV and 0.768 eV in SDC0.25 and SDC3.0, respectively. These values align with previously reported data for ceria-based and proton-conducting electrolytes, indicating that $RHASiO_2$ not only improves densification but also contributes to more efficient charge transport across the electrolyte matrix [22, 23].

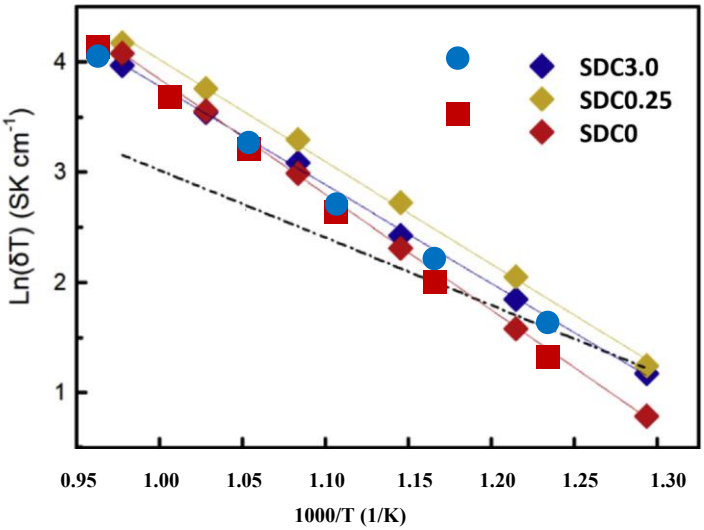

Figure 8: Arrhenius plot (lndtT – 1/T) of different electrolytes measured between 500 and 700 °C

Among the studied compositions, SDC3.0 demonstrated the highest total ionic conductivity within the temperature range of 500–700 °C. At 700 °C, SDC3.0 achieved a conductivity of 2.76 x 10^{-2} $S \cdot cm^{-1}$, outperforming both SDC0.25 (2.07 x 10^{-2} $S \cdot cm^{-1}$) and the undoped SDC0 (1.96 x 10^{-2} $S \cdot cm^{-1}$). The conductivity improvement observed (up to 2.76 × 10^{-2} $S \cdot cm^{-1}$ at 700 °C) is comparable and in some cases superior to reported values for SDC-based electrolytes in the literature, which typically range from 1.0 × 10^{-2} to 2.5 × 10^{-2} $S \cdot cm^{-1}$ at similar temperatures. This confirms the effectiveness of $RHASiO_2$ as a sintering aid. This superior performance is primarily attributed to a significant reduction in grain boundary resistance (Rgb), likely driven by the refined microstructure and increased grain boundary density associated with higher $RHASiO_2$ content

Table 3: Total conductivities (*dt*) at 500 °C, 600 °C and 700 °C and conduction activation energy (Ea) in different electrolytes

Electrolyte	*dt* at 500 °C ($S \cdot cm^{-1}$) x 10^{-2}	*dt* at 600 °C ($S \cdot cm^{-1}$) x 10^{-2}	*dt* at 700 °C ($S \cdot cm^{-1}$) x 10^{-2}	*Ea* (eV)
SDC0	0.59	1.21	1.96	0.898
SDC0.25	0.77	1.34	2.07	0.796
SDC3.0	0.94	1.72	2.76	0.768

Furthermore, SDC3.0 exhibited the lowest conduction activation energy (0.768 eV) among the three compositions, compared to 0.796 eV for SDC0.25 and 0.898 eV for SDC0. The progressive decline in activation energy with increasing $RHASiO_2$ concentration suggests that the $RHASiO_2$ phase not only enhances microstructural properties but also directly contributes to charge transport, thereby improving overall conductivity. Although the bulk resistance (Rb) was observed to increase slightly

with $RHASiO_2$ addition, the substantial drop in Rgb and the reduced activation energy more than compensated for this effect. Consequently, SDC3.0 emerged as the optimal composition, offering the most effective balance of microstructure, activation energy, and conductivity enhancement for high-temperature electrochemical applications.

4. CONCLUSIONS

This study successfully demonstrates the potential of natural $RHASiO_2$ as a sustainable and effective sintering aid for enhancing the structural and electrochemical performance of SDC electrolytes in intermediate-temperature solid oxide fuel cells. TGA confirmed that $RHASiO_2$ incorporation improves thermal stability by reducing total weight loss across all degradation phases, with SDC3.0 showing the most significant resistance to decomposition. Morphological observations via SEM coupled with ImageJ analysis revealed a progressive reduction in porosity, from 4.95 % in pure SDC to 4.58 % in the 3 wt% $RHASiO_2$ composite, confirming improved densification. EIS further highlighted the positive effect of $RHASiO_2$ on electrical properties, particularly grain boundary conductivity. The highest total ionic conductivity of 2.76 x 10^{-2} $S \cdot cm^{-1}$ at 700 °C was achieved by the SDC3.0 composition, which also exhibited the lowest activation energy of 0.768 eV.

Overall, the addition of $RHASiO_2$ not only enhances the microstructural integrity and reduces porosity, but also significantly boosts the ionic conductivity of SDC electrolytes without requiring extreme sintering temperatures. These findings underline $RHASiO_2$ as a promising, eco-friendly, and low-cost sintering additive for the development of high-performance IT-SOFC electrolytes, contributing to the advancement of more sustainable and efficient fuel cell technologies.

Acknowledgements

The author gratefully acknowledges the financial support provided by Ministry of Higher Education Malaysia for providing financial support through the FRGS Grant (FRGS/1/2020/TK0/UTHM/03/18), Malaysian Technical University Network for the financial support provided through the MTUN Grant (MTUN/2023/UTeM-FKP/M00023(UTHM)) and Research Management Centre (RMC), Universiti Tun Hussein Onn Malaysia (UTHM) for managing our research grant.

Author Contributions

All authors contributed toward data analysis, drafting and critically revising the paper and agree to be accountable for all aspects of the work.

Disclosure of Conflict of Interest

The authors have no disclosures to declare.

Compliance with Ethical Standards

The work is compliant with ethical standards.

References

[1] Jaidi, Z., Azmi, M. A., Rahman, H. A., Zakaria, H., Hassan, S., Mahzan, S., Ismail, A., Ariffin, A. M. T., Tukimon, M. F., Yusof, U. A. & Baharuddin, N. A. (2023). Samarium doped ceria (SDC) electrolyte modification by sintering aids addition to reducing sintering temperature: A review. *Jurnal Kejuruteraan*, 35(1), 65–76.

[2] Xu, Q. (2023). Modelling Of High Temperature Methanol-Fuelled Solid Oxide Fuel Cells. (PhD. Thesis, Hong Kong Polytechnic University) pp. 3-6.

[3] Tian, Y., Abhishek, N., Yang, C., Yang, R., Choi, S., Chi, B., Pu, J., Ling, Y., Irvine, J. T. S. & Kim, G. (2022). Progress and potential for symmetrical solid oxide electrolysis cells. *Matter,* 5(2), 482–514.

[4] Jaidi, Z., Azmi, M. A., Mokhtar, M. A., Rahman, H. A., Mahzan, S., Ismail, A. & Ibrahim, M. H. I. (2024). Study of material characterization of samarium doped ceria-rice husk ash silica (SDC-RHASiO2). In Proceedings of the Advanced Materials Characterization Techniques 2022 (AMCT2022), Malaysia, 28–29 Aug 2022.

[5] Jaidi, Z., Azmi, M. A., Rahman, H. A., Tukimon, M. F., Ghani, I. A., Syahmie, M., Shukor, S. A. & Huai, T. K. (2024). The Effect of rice husk ash silica ($RHASiO_2$) composition to the properties of samarium-doped ceria electrolyte. *Malaysian Journal of Microscopy,* 20(1), 328–36.

[6] Hussain, S. & Yangping, L. (2020). Review of solid oxide fuel cell materials: cathode, anode, and electrolyte. *Energy Transitions,* 4, 113–26.

[7] Seo, Y., Minehira, M., Cho, S., Goto, T. & Kondo, Y. (2025). Cold sintering of silicon nitride using surface-amorphous silica. *Journal of Alloys and Compounds,* 1045, 184716

[8] Pravitha, S., Priyanka, S., Devadathan, D. & Raveendran, R. (2026). A review of functional rare earth metal oxides : synthesis strategies, properties, and emerging applications. *Coordination Chemistry Reviews,* 558, 217767.

[9] Wang, T., Li, Q., Liu, X., Bilal, M., Dong, D. & Wang, H. (2025). Nanofabrication technologies for low-temperature solid oxide cells : a comprehensive review of techniques, challenges, and future perspectives. *Energy Reviews*, 4, 100163

[10] Jaidi, Z., Azmi, M. A., Rahman, H. A., Kang, H. T., Yusop, U. A., Zul, M., Ghani, I. A. & Roslan, M. F. (2023). The effect of milling duration to the structural properties of silica from rice husk. *Malaysian Journal of Microscopy,* 19(1), 193–201.

[11] Mennilli, F., Giannetti, L., Ferrario, A. M., Rossi, M., Comodi, G. & Pietra, M. D. (2024). An Electrochemical Impedance Spectroscopy (EIS) analysis of a reversible Solid Oxide Cell (rSOC) for its electrochemical characterisation. *Journal of Physics: Conference Series.* 2893, 012065.

[12] Bashir, Z., Nazir, Z., Nazli, H., Akram, A. & Riaz, S. (2025) Insights into structural , dielectric , and magnetic properties of indium oxide composites. *Solid State Communications*, 404, 116048.

[13] Afzal, S. A., Hussain, F., Siyal, S. H., Javed, M. S., Saleem, M., Imran, M., Assiri, M. A., Bahajjaj, A. A. A., Ghfar, A. A., Al-Anazy, M. M., Ouladsmane, M., Al-Tamrah, S. & Ali, S. (2021). Weight loss during calcination and sintering process of $Na_{0.5}Bi_{0.5}TiO_3$–$Bi_{½}(Mg_{2/3}Nb_{1/3})O_3$ composite lead-free piezoelectric ceramics. *Coatings,* 11(6), 676.

[14] Amran, M., Fediuk, R., Murali, G., Vatin, N., Karelina, M., Ozbakkaloglu, T., Krishna, R. S., Kumar, A. S., Kumar, D. S. & Mishra, J. (2021). Rice husk ash-based concrete composites: A critical review of their properties and applications. *Crystals*, 11(2), 168.

[15] Palacios, A., Navarro-Rivero, M. E., Zou, B., Jiang, Z., Harrison, M. T. & Ding, Y. (2023). A perspective on phase change material encapsulation: Guidance for encapsulation design methodology from low to high-temperature thermal energy storage applications. *Journal of Energy Storage*, 72, 108597.

[16] Elyazed, A. S. A., Ashry, A. G., Edris, A. E., Mousa, A. F., Nassar, M. Y., Adam, M. S. S., Kamoun, E. A., Alfurayj, I., Bakir, E. M. & Abdel-rahman, A. A. (2026). Synthesis of silica / soda lime composite catalyst from rice husk ash for efficient biodiesel production. *Results in Engineering*, 30, 110308.

[17] Muda, R., Ahmad, S., Azmi, M. A., Taib, N. & Taib, H. (2019). Characterisation of silica derived from rice husk ash and nickel oxide at different composition and temperatures. *International Journal of Materials and Product Technology*, 59(2), 91–101.

[18] Abubakar, M., Muthuraja, A., Rajak, D. K., Ahmad, N., Pruncu, C. I., Lamberti, L. & Kumar, A. (2020). Influence of firing temperature on the physical, thermal and microstructural properties of kankara kaolin clay: A preliminary investigation. *Materials,* 13(8), 1872.

[19] Shaari, N. & Kamarudin, S. K. (2019). Current status, opportunities, and challenges in fuel cell catalytic application of aerogels. *International Journal of Energy Research,* 43(7), 2447–2467.

[20] Abdel Rhiem, E., Mohamed, S. G., Barakat, Y. F., Mostafa, M. M., Nada, R. H. & Abdelaziz, S. M. (2023). Corrosion behavior and microstructure of Al–10Zn alloy with nano CuO addition. *Scientific Reports,* 13, 12855.

[21] Ge, F., Liu, S., Zhang, X., Shan, M., Peng, C., Jia, F., Han, J. & Cai, Y. (2023). Effect of grain orientation on microstructure and mechanical properties of FeCoCrNi high-entropy alloy produced via laser melting deposition. *Materials*, 16(17), 5963.

[22] Mishra, S., Choudhary, R. N. P. & Parida, S. K. (2023). Microstructure, dielectric relaxation, optical, and ferroelectric studies of a lead-free double perovskite: $BaLiFeMoO_6$. *Journal of the Korean Ceramic Society*, 60, 310–30.

[23] Karmakar, S. (2024). Impedance Spectroscopy for Electroceramics and Electrochemical System. *Advanced Energy Conversion Materials,* 6, 10–56.

[24] Alotaibi, M. (2022). Oxide ion conductivity, Resistive-switching and Ferroelectricity of Doped-HfO2. (PhD Thesis, University of Sheffield) pp. 66-75.